

NUCLEAR LUMINOSITIES AND RADIO LOUDNESS OF SEYFERT NUCLEI

LUIS C. HO

The Observatories of the Carnegie Institution of Washington,
813 Santa Barbara St., Pasadena, CA 91101

AND

CHIEN Y. PENG

Steward Observatory, Univ. of Arizona, Tucson, AZ 85721

To appear in The Astrophysical Journal.

ABSTRACT

Historically, Seyfert nuclei have been considered to be radio-quiet active galactic nuclei (AGNs). We question this widely held assumption by showing that the distribution of the radio-to-optical luminosity ratio, $R \equiv L_\nu(6 \text{ cm})/L_\nu(B)$, when properly measured for the *nuclear* component, places the majority of type 1 Seyfert nuclei in the category of radio-loud AGNs, defined here as objects with $R \geq 10$. This result is further strengthened by strong correlations found between radio power and optical continuum and emission-line luminosities, as has been established previously for more powerful AGNs. We also present a new calibration of the relation between optical continuum and Balmer emission-line luminosities valid in the regime of low-luminosity AGNs.

Subject headings: galaxies: active — galaxies: nuclei — galaxies: Seyfert — radio continuum: galaxies

1. INTRODUCTION

Active galactic nuclei (AGNs) nearly universally emit synchrotron radiation at radio wavelengths. The character of the radio emission shows tremendous diversity, ranging from relatively simple structures such as parsec-scale central cores, to well collimated jets and lobes extending over hundreds of kpc. Historically, one of the most notable attributes of AGNs is the apparent bimodal distribution of their strength of radio emission (Strittmatter et al. 1980; Sramek & Weedman 1980). Optically selected AGNs seem to fall into one of two categories — “radio loud” or “radio quiet” — the dividing line generally set by the relative monochromatic luminosities at radio and optical wavelengths. A widely adopted convention (or some closely related variant) is $R \equiv L_\nu(6 \text{ cm})/L_\nu(B)$, with the boundary between the two radio classes set at $R = 10$ (Visnovsky et al. 1992; Stocke et al. 1992; Kellermann et al. 1994). Miller, Peacock, & Mead (1990) advocate an alternative criterion based on the radio luminosity alone, a limit set to $P_{6\text{cm}} \approx 10^{25} \text{ W Hz}^{-1} \text{ sr}^{-1}$. The majority of optically selected quasars are radio quiet, with only $\sim 10\%$ – 20% qualifying as radio loud, based on either of the above criteria (e.g., Kellermann et al. 1989; Visnovsky et al. 1992; Hooper et al. 1995). Some recent studies using radio selected samples of quasars have questioned the bimodality in the distribution of R (Wadadekar & Kembhavi 1999; White et al. 2000).

The actual shape of the R distribution notwithstanding, the fraction of radio-loud AGNs tends to increase for the optically most luminous objects (e.g., Miller et al. 1990). At low redshift, where high-resolution optical and near-infrared images are now readily available, radio-loud quasars preferentially inhabit luminous, massive, early-type galaxies, whereas the hosts of radio-quiet quasars span a wider range of morphological types (e.g., McLure et al. 1999; Hamilton, Casertano, & Turnshek

2001). Radio galaxies themselves have long been known to be predominantly giant ellipticals (e.g., Matthews, Morgan, & Schmidt 1964; Zirbel 1996; de Vries et al. 2000). Within this backdrop, Seyfert galaxies, which are generally considered to be the low-luminosity extension of the quasar phenomenon, traditionally have been regarded as radio-quiet objects. This perception perhaps has been reinforced further by the apparent correlation between radio loudness and host galaxy morphology, since most Seyfert nuclei reside in disk (spiral and lenticular) systems (e.g., Adams 1977; Yee 1983; MacKenty 1990; Ho, Filippenko, & Sargent 1997b). By virtue of their proximity, a high percentage of Seyfert galaxies are detectable as radio sources (e.g., de Bruyn & Wilson 1978; Ulvestad & Wilson 1984a, 1984b, 1989; Edelson 1987; Rush, Malkan, & Edelson 1996; Ho & Ulvestad 2001). Nonetheless, their modest radio luminosities ($P_{6\text{cm}} \approx 10^{19} - 10^{22} \text{ W Hz}^{-1}$) and their accompanying small radio-to-optical luminosity ratios have cemented the notion that Seyferts are radio-quiet objects. In phenomenological classifications of AGNs, type 1 and type 2 Seyferts often are viewed as the radio-quiet analogs of broad-line and narrow-line radio galaxies, respectively (e.g., Osterbrock 1984; Lawrence 1987; Blandford 1990; Peterson 1997; Krolik 1998). Laor (2000) explicitly argues that the bulges of spiral galaxies cannot produce radio-loud AGNs.

Extending the R parameterization to Seyferts, however, is not straightforward. In the case of quasars, the active *nucleus* significantly outshines the underlying galaxy at optical, and often also at radio, wavelengths. Consequently, R , computed from the integrated emission, faithfully represents a quantity germane to the AGN. The situation for Seyferts is more complicated. Once an object is recognized as a Seyfert *galaxy*, the underlying host obviously contributes appreciably to the integrated optical light of the system. Most Seyfert nuclei are found in bulge-dominated, relatively luminous ($\sim L^*$) galaxies; typically,

$M_{B_T} \approx -21 \pm 1$ mag (e.g., Ho et al. 1997b)¹. The optical luminosities of the nuclei, on the other hand, span an enormous range. Given the tremendous range of brightness contrast between the nucleus and the bulge, in general the optical luminosity of Seyfert nuclei can be characterized properly only with measurements which sufficiently resolve the nuclear region. A similar caveat applies to the radio data. The disks of spiral galaxies emit synchrotron radio emission at a level which easily rivals the nuclear emission. Normal early-type spirals, for instance, have typical 20 cm powers of 10^{20} – 10^{22} W Hz⁻¹ (Hummel 1981; Condon 1987), within the range emitted by the nucleus. In general, therefore, the AGN component of the radio signal in Seyferts can be isolated reliably only using high-resolution, interferometric data.

The primary goal of this paper is to reexamine the conventional claim that Seyfert nuclei, and by implication their spiral host galaxies, are mainly radio quiet. We use high-resolution optical and radio continuum measurements to show that the nuclear values of R in the majority of Seyferts place them in the category of radio-loud objects. Our data also furnish insights into the physical relationship between radio power and optical continuum and emission-line luminosities. We suggest that the fueling of radio jets may be closely linked with the disk accretion rate. Lastly, we present a new calibration of the relation between optical continuum and Balmer emission-line luminosities for type 1 AGNs.

2. THE SAMPLE

For the purposes of this study, we choose only objects classified as Seyfert 1 nuclei, which are believed to be relatively unobscured sources and hence provide the most direct comparison with quasars. We consider a sample drawn from two optical spectroscopic surveys of nearby galaxies. Ho, Filippenko, & Sargent (1995) surveyed a nearly complete sample of 486 bright ($B_T \leq 12.5$ mag), northern ($\delta > 0^\circ$) galaxies using the Palomar 5-m telescope, from which they derived a sensitive catalog of emission-line nuclei, including a comprehensive list of nearby AGNs (Ho et al. 1997a, 1997b, 1997c). The Palomar survey contains 49 Seyfert galaxies², 21 of type 1 and 28 of type 2, most of which have low luminosities (median $L_{H\beta} = 5 \times 10^{39}$ erg s⁻¹) and are nearby (median $D = 20$ Mpc). As discussed by Ho et al. (1997b) and Ho & Ulvestad (2001), the Palomar Seyfert sample is the most complete and least biased available. One drawback of this sample, however, is that it contains relatively few objects on the upper end of the luminosity function.

We therefore supplement the Palomar sample with Seyferts derived from the CfA redshift survey (Huchra et al. 1983). Spectra were acquired for 2399 galaxies with Zwicky magnitudes ≤ 14.5 that lie within $\delta \geq 0^\circ$ and $b_{II} \geq 40^\circ$ or $\delta \geq -2^\circ.5$ and $b_{II} \leq -30^\circ$. Huchra & Burg (1992) compiled a list of 49 Seyfert galaxies, the spectroscopic classifications of which were subsequently refined by Osterbrock & Martel (1993). According to the classifications of Osterbrock & Martel, the CfA sample contains

33 Seyfert 1s and 15 Seyfert 2s; one object (Mrk 789) was judged to be a starburst galaxy. The median distance of the CfA Seyferts is ~ 80 Mpc. Ho & Ulvestad (2001; see § A.2) argue that the CfA Seyfert sample suffers from complex selection effects. In the case of Seyfert 1s, the primary effect is a bias against faint, intrinsically weak nuclei. As an illustration of the level of incompleteness, we note that 19 out of the 21 Seyfert 1s from the Palomar sample formally fall within the selection boundaries of the CfA survey, but only nine (43%) were recognized as Seyfert 1s by Huchra & Burg; all nine objects have very prominent broad emission lines. Thus, the samples of Seyfert 1 nuclei from the Palomar and CfA surveys complement one another, although the combined sample in itself cannot be regarded as complete. Fortunately, this limitation does not affect the major results of this study, but we caution against other applications of the data where sample completeness matters (e.g., derivation of luminosity functions). Our final sample, summarized in Table 1, consists of 45 objects: 21 from the Palomar survey, 33 from the CfA survey, and nine common to both.

3. THE DATA

3.1. Palomar and CfA Seyfert 1 Nuclei

The radio data come primarily from two sources. Kukula et al. (1995) imaged the CfA sample at 3.6 cm (8.4 GHz) using the Very Large Array (VLA) in its A and C configurations; the resulting angular resolutions are $\sim 0''.25$ and $\sim 2''.5$, respectively. They did not observe Mrk 471 because it was inadvertently omitted from the original list of Huchra & Burg (1992). We used the data of Ulvestad (1986) for this object. The radio properties of the full Palomar sample were recently investigated by Ho & Ulvestad (2001). They obtained scaled-array 6 cm (4.9 GHz) and 20 cm (1.4 GHz) continuum images with the VLA at a resolution of $\sim 1''$. Eighty-five percent of the objects were detected at 6 cm above a 3σ threshold of ~ 0.12 mJy beam⁻¹. The signal-to-noise ratio of the Kukula et al. maps is slightly lower than that of Ho & Ulvestad, but the two surveys are otherwise quite compatible in terms of sensitivity and resolution. Table 2 gives 6 cm monochromatic radio powers for the combined sample, derived from the observed flux densities assuming isotropic emission; the listed values pertain to the integrated emission from all components associated with the AGN. The 3.6 cm data of Kukula et al. (1995) were extrapolated³ to the fiducial wavelength of 6 cm assuming $f_\nu \propto \nu^{\alpha_r}$, with $\alpha_r = -0.5$, the median spectral index between 6 and 20 cm found by Ho & Ulvestad (2001). We adopt the results of Ho & Ulvestad (2001) for the few objects that overlap between the two samples. Altogether, 93% (42/45) of the objects have radio detections, which range from ~ 0.5 mJy to 21 Jy, with a median value of ~ 6 mJy.

High-resolution ($\sim 0''.1$) optical images for the majority (37/45) of the objects are available from the *Hubble Space Telescope* (*HST*) studies of Nelson et al. (1996), Malkan, Gorjian, & Tam (1998), and Ho et al. (2001b, in prepara-

¹Throughout this paper, we adopt a Hubble constant of $H_0 = 75$ km s⁻¹ Mpc⁻¹ and a deceleration parameter of $q_0 = 0.5$.

²Ho et al. (1997a) list a total of 52 Seyferts (22 type 1, 30 type 2), but three of these have $\delta < 0^\circ$ and so formally do not belong to the complete sample. We include intermediate-type objects (Osterbrock 1981) in the type 1 class.

³Although 6 cm data have been published for many of the CfA Seyferts, we prefer to utilize the 3.6 cm database of Kukula et al. (1995) for the sake of homogeneity.

TABLE 1: GLOBAL PROPERTIES OF THE SEYFERT SAMPLE

Galaxy Name (1)	Alternate Name (2)	Sample (3)	Seyfert Class (4)	Hubble Type (5)	cz (km s ⁻¹) (6)	D (Mpc) (7)	A_B^{Gal} (mag) (8)	M_{B_T} (mag) (9)	$\log P_{6\text{cm}}^{\text{tot}}$ (W Hz ⁻¹) (10)	Ref. (11)
I Zw 1	UGC 545	C	1.0	S?	18116	241.6	0.28	-22.83	22.34	1
Mrk 205		C	1.0	SBab	20978	279.7	0.18	-22.91	22.23	1
Mrk 231	UGC 8058	C	1.0	Sc?	12287	163.8	0.04	-21.70	23.95	1
Mrk 279	UGC 8823	C	1.5	S0	9129	121.7	0.07	-20.92	22.11	1
Mrk 334	UGC 6	C	1.8	Pec	6605	88.1	0.20	-20.55	22.02	1
Mrk 335	PG 0003+199	C	1.0	S0/a	7757	103.4	0.15	-21.48	21.57	1
Mrk 471	UGC 9214	C	1.8	SBa	10263	136.8	0.04	-21.18	21.73	2
Mrk 530	NGC 7603	C	1.5	Sb:	8691	115.9	0.20	-21.48	22.27	1
Mrk 590	NGC 863	C	1.2	Sa:	7891	105.2	0.16	-21.42	22.00	1
Mrk 744	NGC 3786	C	1.8	SABa	2737	41.6	0.10	-19.96	21.16	1
Mrk 766	NGC 4253	C	1.5	SBa:	3836	51.7	0.08	-19.65	21.69	1
Mrk 817	UGC 9412	C	1.5	SBc	9430	125.7	0.03	-21.03	21.99	1
Mrk 841	IRAS 15015+1037	C	1.5	E	10921	145.6	0.13	-21.95	22.22	1
Mrk 993	UGC 987	C	1.5	SAB0/a	4625	61.7	0.26	-19.82	20.94	1
Mrk 1243	NGC 3080	C	1.0	Sa	10602	141.4	0.13	-21.56
NGC 1275	3C 84, Perseus A	P	1.5	Pec	5260	70.1	0.70	-22.29	25.46	3
NGC 2639		P	1.9	Sa:?	3282	42.6	0.10	-20.69	21.90	3
NGC 3031	M81	P	1.5	Sab	-37	3.6	0.35	-20.24	20.32	3
NGC 3227		P/C	1.5	SABa	1156	20.6	0.10	-20.57	21.25	1
NGC 3516		P/C	1.2	SB0:	2624	38.9	0.18	-20.63	21.28	1
NGC 3982		P	1.9	SABb:	1105	17.0	0.06	-19.43	20.92	3
NGC 4051		P/C	1.2	SABbc	720	17.0	0.06	-20.38	20.60	1
NGC 4138		P	1.9	S0	924	17.0	0.06	-19.05
NGC 4151		P/C	1.5	SABab:	992	20.3	0.12	-20.16	21.79	1
NGC 4168		P	1.9	E2	2283	16.8	0.16	-19.17
NGC 4235		P/C	1.2	Sa	2404	35.1	0.08	-20.19	20.93	1
NGC 4258	M106	P	1.9	SABbc	450	6.8	0.07	-20.13	21.23	3
NGC 4388		P	1.9	Sb:	2517	16.8	0.14	-19.51	21.18	1
NGC 4395		P/C	1.8	Sm:	320	2.6	0.07	-16.51	18.87	4
NGC 4565		P	1.9	Sb?	1225	9.7	0.07	-19.58	20.80	4
NGC 4579	M58	P	1.9	SABb	1521	16.8	0.18	-20.82	21.26	3
NGC 4639		P	1.0	SABbc	1006	16.8	0.12	-19.00	20.36	5
NGC 5033		P/C	1.5	Sc	877	18.7	0.05	-20.66	21.22	1
NGC 5252		C	1.9	S0	6926	92.3	0.14	-20.93	22.27	1
NGC 5273		P/C	1.5	S0	1054	21.3	0.04	-19.24	20.04	1
NGC 5548	Mrk 1509	P/C	1.5	S0/a	5140	68.5	0.09	-20.97	21.89	1
NGC 5674		C	1.9	SABc	7442	99.2	0.15	-21.44	22.05	1
NGC 5940		C	1.0	SBab	10160	135.5	0.18	-21.52	21.98	1
NGC 6104		C	1.5	S	8397	111.9	0.08	-21.12	21.62	1
NGC 7469	Mrk 1514	C	1.0	SABa	4790	63.9	0.30	-21.32	22.54	1
NGC 7479		P	1.9	SBc	2378	32.4	0.48	-21.43	21.69	3
UGC 524	IRAS 00488+2907	C	1.0	SBb	10763	143.5	0.27	-21.66	21.84	1
UGC 1395	UM 146	C	1.9	Sb	5208	69.4	0.32	-20.35	21.76	1
UGC 8621	IRAS 13354+3924	C	1.8	S?	6023	80.3	0.03	-20.28	21.00	1
UGC 12138	IRAS 22377+0747	C	1.8	SBa	7487	99.8	0.37	-21.12	21.72	1

NOTE.— Col. (1) Galaxy name. Col. (2) Alternate name. Col. (3) Seyfert sample, where “C” refers to CfA, “P” refers to Palomar, and “P/C” means common to both. Col. (4) Seyfert classification as given in Ho et al. 1997a for the Palomar sample and in Osterbrock & Martel 1993 for the CfA sample. Col. (5) Hubble type as given in Ho et al. 1997a for the Palomar sample and in the NASA/IPAC Extragalactic Database (NED) for the CfA sample. Col. (6) Heliocentric velocity as given in Ho et al. 1997a for the Palomar sample and in Huchra & Burg 1992 for the CfA sample. Col. (7) Adopted distance as given in Tully 1988 for $D < 40$ Mpc (except for NGC 3031 and NGC 4395), and otherwise derived using cz and $H_0 = 75$ km s⁻¹ Mpc⁻¹. Col. (8) Galactic extinction in the B band, as given in NED, which is estimated from Schlegel, Finkbeiner, & Davis 1998 assuming $A_V = 3.1E(B - V)$ and the extinction curve of Cardelli, Clayton, & Mathis 1989. Col. (9) Total absolute B magnitude of the galaxy, corrected for Galactic extinction, based on apparent magnitudes given in Ho et al. 1997a for the Palomar sample and in NED for the CfA sample (except for Mrk 205 and Mrk 841, which come from Huchra & Burg 1992). Col. (10) Total 6 cm power obtained from low-resolution (beam $\gtrsim 1'$ in most cases) observations; in a few cases where 6 cm data were unavailable we extrapolated measurements from other wavelengths assuming $f_\nu \propto \nu^{-0.5}$. Col. (11) Reference for the radio data.

REFERENCES.— (1) Rush et al. 1996, resolution 1.5; (2) Meurs & Wilson 1984, resolution 25'', extrapolated from 20 cm; (3) Becker, White, & Edwards 1991, resolution 3.5; (4) Condon 1987, resolution 1', extrapolated from 20 cm; (5) Niklas, Klein, & Wielebinski 1995, resolution 1.2, extrapolated from 2.8 cm.

ration), or from the *HST* data archives. Twenty-seven of the objects were observed with the Wide Field Planetary

Camera 2 (WFPC2), and 10 with the Wide Field Planetary Camera 1 (WFPC1), using a variety of medium-

TABLE 2: NUCLEAR OPTICAL AND RADIO PROPERTIES

Galaxy Name (1)	m^{nuc} (mag) (2)	Detector/ Filter (3)	Note (4)	m_B^{nuc} (mag) (5)	M_B^{nuc} (mag) (6)	$\log L_{H\beta}$ (erg s^{-1}) (7)	$\log L_{[\text{O III}]}$ (erg s^{-1}) (8)	Ref. (9)	$\log S_{6\text{cm}}$ (mJy) (10)	$\log P_{6\text{cm}}$ (W Hz^{-1}) (11)	$\log R$ (12)
I Zw 1	15.59	WFPC1/F555W	a	15.72	-21.47	41.59	42.15	1	0.47	22.31	0.04
Mrk 205	16.46	WFPC2/F814W	a	16.41	-21.00	41.79	42.31	1	0.19	22.16	0.08
Mrk 231	14.28	WFPC2/F814W	a	14.23	-21.88	41.88	42.30	1	2.47	23.98	1.54
Mrk 279	b,c	14.94	-20.55	41.42	41.81	2	0.81	22.06	0.16
Mrk 334	b,c	>15.04	>-19.89	40.73	40.56	1	0.99	21.96	>0.33
Mrk 335	15.67	WFPC1/F785LP	a	17.05	-18.18	41.52	42.14	2	0.47	21.57	0.62
Mrk 471	<18.67	WFPC2/F606W	a,d	<18.93	<-16.79	40.66	40.57	1	-0.00	21.35	<0.95
Mrk 530	17.87	WFPC1/F785LP	a	19.25	-16.27	40.74	41.26	1	1.04	22.24	2.06
Mrk 590	17.43	WFPC1/F785LP	a	18.81	-16.46	40.91	40.96	2	0.76	21.88	1.62
Mrk 744	b,c	15.64	-17.56	40.39	39.89	1	0.62	20.94	0.24
Mrk 766	15.70	WFPC1/F785LP	a	17.08	-16.57	41.36	40.79	2	1.13	21.63	1.33
Mrk 817	16.34	WFPC1/F785LP	a	17.72	-17.81	41.40	41.89	2	0.74	22.02	1.21
Mrk 841	16.53	WFPC1/F785LP	a	17.91	-18.04	41.85	42.27	1	-0.08	21.32	0.43
Mrk 993	20.15	WFPC2/F606W	a	20.41	-13.80	40.23	39.46	1	0.29	20.95	1.75
Mrk 1243	e	14.49	-21.39	40.54	41.27	1	<-0.41	<20.97	<-1.27
NGC 1275	15.85	WFPC2/F450W	a	16.40	-18.53	41.85	41.32	3	4.32	25.09	4.00
NGC 2639	>23.29	WFPC2/F606W	a	>23.55	>-9.70	40.45	39.90	3	2.26	22.60	>5.04
NGC 3031	16.04	WFPC2/F547M	a,d	16.40	-11.73	38.67	38.61	4	1.97	20.16	1.79
NGC 3227	15.30	WFPC2/F547M	a	15.66	-16.01	40.54	40.13	2	1.50	21.20	1.12
NGC 3516	15.56	WFPC2/F547M	a	15.92	-17.21	41.00	41.18	2	1.09	21.34	0.78
NGC 3982	19.19	WFPC2/F606W	a,d	19.45	-11.76	39.86	38.53	3	0.62	20.16	1.78
NGC 4051	15.89	WFPC1/F547M	a	16.24	-14.97	40.15	39.96	2	1.00	20.54	0.87
NGC 4138	>21.30	WFPC2/F547M	f	>21.66	>-9.55	38.76	37.99	3	-0.11	19.43	>1.93
NGC 4151	12.12	WFPC2/F547M	a	12.48	-19.18	41.81	41.38	2	2.14	21.84	0.49
NGC 4168	>23.98	WFPC2/F547M	f	>24.34	>-6.94	37.96	37.39	3	0.71	20.24	>3.78
NGC 4235	17.56	WFPC2/F547M	f	17.92	-14.89	39.58	40.02	2	0.76	20.93	1.30
NGC 4258	>20.70	WFPC2/F547M	f	>21.06	>-8.17	38.77	37.77	3	0.55	19.29	>2.34
NGC 4388	18.87	NIC1/F160W	a,g	18.10	-13.17	40.26	39.16	2	1.66	21.19	2.24
NGC 4395	17.91	WFPC2/F450W	a	18.46	-8.69	38.14	37.35	3	0.10	18.01	0.85
NGC 4565	19.26	WFPC2/F450W	a	19.81	-10.19	38.25	37.31	3	0.43	19.48	1.72
NGC 4579	18.13	WFPC2/F547M	a	18.49	-12.81	39.48	38.99	3	1.63	21.16	2.35
NGC 4639	19.91	WFPC2/F547M	a	20.27	-10.97	38.45	39.07	3	-0.23	19.30	1.23
NGC 5033	16.52	WFPC2/F547M	a	16.88	-14.53	39.37	39.25	3	1.38	21.00	1.51
NGC 5252	19.90	WFPC2/F336W	a	20.74	-14.23	41.40	40.63	6	1.09	22.10	2.72
NGC 5273	17.81	WFPC2/F547M	a	18.17	-13.51	39.09	38.06	2	0.25	19.98	0.90
NGC 5548	15.60	WFPC1/F785LP	a	16.98	-17.29	41.54	41.70	2	1.09	21.84	1.24
NGC 5674	18.96	WFPC2/F606W	a,h	19.22	-15.92	41.23	40.66	6	<-0.21	<20.86	<0.82
NGC 5940	17.46	WFPC2/F606W	a,d	17.72	-18.12	40.95	41.39	7	-0.13	21.21	0.28
NGC 6104	18.90	WFPC2/F606W	a	19.16	-16.17	<-0.46	<20.72	<0.57
NGC 7469	15.16	WFPC1/F785LP	a	16.54	-17.78	41.55	41.79	2	1.74	22.43	1.64
NGC 7479	>22.04	WFPC2/F569W	a,i	>22.36	>-10.67	39.31	38.72	3	1.05	21.15	>3.20
UGC 524	e	15.36	-20.70	0.16	21.55	-0.41
UGC 1395	19.24	WFPC2/F606W	a	19.50	-15.03	40.65	39.99	2	0.86	21.62	1.93
UGC 8621	e	13.85	-20.70	-0.10	20.78	-1.17
UGC 12138	b,c	>15.56	>-19.80	41.59	41.41	6	0.53	21.61	>0.01

NOTE.— Col. (1) Galaxy name. Col. (2) Apparent magnitude (in STMAG system) of the nucleus as measured from *HST* images. Col. (3) *HST* detector and filter. Col. (4) Notes for the *HST* data: (a) data from the *HST* archive; (b) *HST* image from Malkan et al. 1998 unusable because of severe saturation; (c) ground-based spectrophotometry (Mrk 279: Stirpe et al. 1994; Mrk 334 and UGC 12138: Cruz-González et al. 1994; Mrk 744: Goodrich & Osterbrock 1983); (d) partly saturated; (e) optical flux density estimated from X-ray data of Della Ceca et al. 1990 (see text); (f) from Ho et al. 2001b, in preparation; (g) NICMOS F160W (*H* band) image; (h) nucleus resolved; (i) pointlike nucleus weak or absent. Col. (5) Estimated apparent *B* magnitude (in Vega system) of the nucleus assuming $f_\nu \propto \nu^{-1.0}$. Col. (6) Absolute *B* magnitude of the nucleus, corrected for Galactic extinction, as given in col. (8) of Table 1. Col. (7) $H\beta$ (narrow + broad components) luminosity, corrected for Galactic extinction. Col. (8) $[\text{O III}] \lambda 5007$ luminosity, corrected for Galactic extinction. Col. (9) Reference for line luminosities. Col. (10) 6 cm flux density of the AGN component as given in Ho & Ulvestad 2001 for the Palomar sample and in Kukula et al. 1995 for the CfA sample (except for Mrk 471, which comes from Ulvestad 1986); we extrapolated the 3.6 cm data of Kukula et al. to 6 cm assuming $f_\nu \propto \nu^{-0.5}$. Col. (11) 6 cm power of the AGN component. Col. (12) Ratio of the nuclear luminosities in the radio to the optical *B* band, defined as $R \equiv L_\nu(6 \text{ cm})/L_\nu(B)$.

REFERENCES.— (1) Dahari & De Robertis 1988; (2) Whittle 1992a; (3) Ho et al. 1997a, 1997c; (4) Ho et al. 1996; (5) Filippenko & Sargent 1989; (6) Cruz-González et al. 1994; (7) Morris & Ward 1988.

band and broad-band filters (see Table 2). It is difficult to obtain accurate photometry of faint nuclei at optical wavelengths because the inner brightness distributions of bulges are both bright and sharply peaked (Phillips et al.

1996; Carollo et al. 1997; Ho et al. 2001b, in preparation). Even at *HST* resolution, it is often nontrivial to disentangle the nucleus from the light of the inner bulge in the presence of complex fine structures (dust lanes, nuclear

spirals, star clusters) invariably present, or to properly take into account the effects of the telescope point-spread function. All the *HST* images, including those of Nelson et al. and Malkan et al. (neither of whom published photometry of the nuclei), were analyzed using GALFIT, a program for galaxy image decomposition developed by Peng et al. (2001, in preparation). In brief, GALFIT fits to the observed image a two-dimensional model for the light distribution consisting of analytic functions for the bulge (“Nuker,” Sérsic, and exponential profiles; details given in Peng et al. 2001, in preparation) plus an additional point source for the nucleus, convolved with an appropriate synthetic point-spread function. Applications of this method to *HST* images of nearby galaxies are given in Ravindranath et al. (2001) and Ho et al. (2001b, in preparation).

For the purposes of this study, we are interested only in obtaining luminosities for the nuclei, and we omit further discussion of the photometric properties of the galaxy bulges. The observed magnitudes are in the STMAG system, defined such that $m_{\text{STMAG}} = -2.5 \log f_{\lambda} - 21.1$, where f_{λ} , in units of $\text{erg s}^{-1} \text{cm}^{-2} \text{\AA}^{-1}$, is constant with wavelength (Holtzman et al. 1995). To facilitate comparison within our sample, and also with quasar samples, we convert the magnitudes to the *B* band in the Vega system, assuming $f_{\nu} \propto \nu^{\alpha_o}$, with $\alpha_o = -1.0$, a typical spectrum for the optical featureless continuum of Seyfert 1 nuclei (e.g., Ward et al. 1987). The conversion factors were calculated using SYNPHOT within STSDAS in IRAF⁴.

Nuclear magnitudes for the remaining eight objects were obtained from more heterogeneous sources, in the following manner. The only *HST* image available for NGC 4388 was taken with NICMOS in the F160W filter (1.6 μm , *H* band); this image was analyzed in the same manner as the optical images, as described by Ravindranath et al. (2001). Ground-based optical spectrophotometry exists for four galaxies: Mrk 279, Mrk 334, Mrk 744, and UGC 12138. Although not ideal (the data were typically acquired with 2”–4” apertures), these observations do give a rough characteristic measurement of the central luminosity of the objects, which is certainly preferable to no correction at all for host-galaxy emission. In any case, the contamination from the host, as judged by the depth of the stellar absorption lines, appears to be quite small for Mrk 279 and Mrk 744. The optical flux densities were converted to *B*-band magnitudes, again using an $\alpha_o = -1.0$ spectrum and SYNPHOT. Finally, for three objects (Mrk 1243, UGC 524, and UGC 8621) we could only locate soft X-ray measurements from the catalog of Della Ceca et al. (1990). We converted the observed count rates to a flux density at 2 keV assuming a power-law spectrum with an energy index of $\alpha_x = -0.7$, as normally seen in type 1 Seyferts (e.g., Nandra et al. 1997). Next, we estimated the near-ultraviolet flux density using a spectral index of $\alpha_{ox} = -1.2$ between 2500 \AA and 2 keV, again a value typical of Seyfert 1s (Mushotzky & Wandel 1989). And

lastly, the *B*-band flux density was obtained by extrapolation from an $\alpha_o = -1.0$ spectrum.

A portion of our analysis will make use of optical emission-line luminosities. We utilize the [O III] $\lambda 5007$ and $H\beta$ (narrow plus broad components) lines, the former to represent emission arising from the narrow-line region (NLR) and the latter from the NLR and broad-line region (BLR). Both are presumed to be predominantly photoionized and hence trace reprocessed continuum emission. In order to minimize systematic errors in the line luminosities due to aperture effects, we have restricted selection of the data to a few well documented, homogeneous sources. Whenever possible we have given preference to the catalog of Whittle (1992a), who has carefully assembled reliable line measurements, followed by the Palomar catalog of Ho et al. (1997a). Markarian Seyferts not included in Whittle’s work were usually found in the compilation of Dahari & De Robertis (1988).

The photometric quantities of the sample are collected in Tables 1 and 2. The absolute magnitudes have been corrected for Galactic extinction but not for internal extinction. In the case of the integrated magnitudes, we have refrained from correcting them to face-on inclination because in some cases the Hubble types and inclinations of the galaxies are poorly known. And although measurements of the narrow-line Balmer decrement are available for most of the nuclei, we have chosen not to apply reddening corrections to the nuclear optical continuum and line luminosities. The continuum light of the nucleus in general may experience a different amount of extinction compared to the emission-line gas. In any case, the correction is modest and will not affect our main conclusions. Using the data from Ho et al. (1997a), we find that the Palomar objects have a median Balmer decrement of $H\alpha/H\beta = 3.7$. For an intrinsic ratio of $H\alpha/H\beta = 3.1$ (Halpern & Steiner 1983; Gaskell & Ferland 1984) and the Galactic extinction law of Cardelli, Clayton, & Mathis (1989), $A_B \approx 0.7$ mag, which is comparable to other sources of systematic uncertainties (§ 3.3).

3.2. Palomar-Green Quasars

Our analysis will make frequent comparisons of the Seyfert sample with optically selected “type 1” AGNs of higher luminosity. For this purpose we have chosen the well studied Palomar-Green (PG) sample of quasars (Schmidt & Green 1983; Green, Schmidt, & Liebert 1986). We limit the PG sample to the 87 objects with $z < 0.5$, since this subset has received the most detailed spectroscopic follow-up work. The radio and optical continuum data come from Kellermann et al. (1989). Boroson & Green (1992)⁵ supply equivalent-width measurements for $H\beta$ and [O III]; we obtained the corresponding line luminosities by combining the equivalent widths with the optical monochromatic continuum luminosities of Kellermann et al., properly extrapolated with $\alpha_o = -1.0$. All distance-dependent quantities were transformed to our

⁴IRAF is distributed by the National Optical Astronomy Observatories, which are operated by the Association of Universities for Research in Astronomy, Inc., under cooperative agreement with the National Science Foundation.

⁵The subsample of PG quasars in the study of Boroson & Green (1992) was also independently investigated spectroscopically by Miller, Rawlings, & Saunders (1993). The study of Miller et al. employed a wider slit than that of Boroson & Green, so in principle the former achieved higher photometric accuracy than the latter, at the expense of somewhat degraded spectral resolution. We have chosen to adopt Boroson & Green’s measurements because these authors accounted for the effects of contamination by Fe II emission, which we deem to be important. Miller et al. indicate that on average the [O III] fluxes of Boroson & Green may have been underestimated by 0.29 dex.

adopted cosmological parameters of $H_0 = 75 \text{ km s}^{-1} \text{ Mpc}^{-1}$ and $q_0 = 0.5$.

3.3. Error Estimates

We do not list errors explicitly for the photometric quantities because in most cases they are dominated by systematic uncertainties which are hard to quantify for each object individually. Here we briefly assess their likely magnitude and their impact on our analysis. Representative error bars appear in the figures later shown in the paper. We assume, for simplicity, that distance errors can be neglected, although this is not well justified for the nearest galaxies whose distances can be rather uncertain.

1. The formal errors of the radio flux densities are generally quite small, dominated by the $\sim 5\%$ uncertainty in the absolute flux scale (see, e.g., Ho & Ulvestad 2001). There is usually little ambiguity in assigning the proper component for the AGN. For the most part, the radio images of Kukula et al. (1995) and Ho & Ulvestad (2001) reveal relatively simple structures, usually consisting of a single, centrally dominant core, which is occasionally accompanied by linear features plausibly associated with plasma outflows. The cores are compact and generally unresolved or barely resolved at resolutions of $\lesssim 1''$. We explicitly assume that all of the emission from the compact core and linear features can be attributed to the AGN, with zero contribution from stellar sources. In spiral galaxies, the integrated centimeter-wave radiation from H II regions and supernova remnants can be significant, but on arc-second scales the radio emission of objects classified as H II or starburst nuclei tends to be diffuse and usually extended along the optical disk (e.g., Condon et al. 1982; Filho, Barthel, & Ho 2000). One cannot rule out that the radio emission might arise from a compact starburst (e.g., Condon et al. 1991), but we regard this possibility to be unlikely for our objects since their optical spectra, measured on comparable scales, by definition are classified as broad-lined AGNs, not starbursts. Variability poses a potentially much more serious problem; however, little is known about the radio variability properties of Seyferts. The handful of objects which have been monitored display intensity fluctuations at centimeter wavelengths ranging from $\sim 30\%$ (NGC 5548; Wrobel 2000) to $\sim 100\%$ (M81; Ho et al. 1999) over timescales of months. We choose 0.2 dex as a fiducial uncertainty for the radio powers. Since the nuclear component of the 6 cm emission can be a significant fraction of the total (Fig. 1), this error estimate may be appropriate for both the nuclear and integrated powers.

2. Several sources of errors can potentially affect the nuclear continuum magnitudes. (1) Even with *HST* resolution, it is in practice very difficult to reliably measure nuclei fainter than $m_V \approx 19\text{--}20$ mag superposed on the intrinsically cuspy cores of bright galaxies, because the inner light profile of the bulge blends smoothly with the weak point source. The majority of the nuclei are brighter than this, however, and the simulations of Peng et al. (2001, in preparation) suggest that GALFIT can extract nuclear magnitudes to an accuracy of $\pm 0.2\text{--}0.3$ mag for galaxies similar to the ones considered here. (2) We use a single $f_\nu \propto \nu^{-1}$ spectrum to extrapolate all the continuum measurements to the *B* band. If we allow the optical power-law slope to vary by as much as $\Delta\alpha_o = \pm 1$, sufficient to

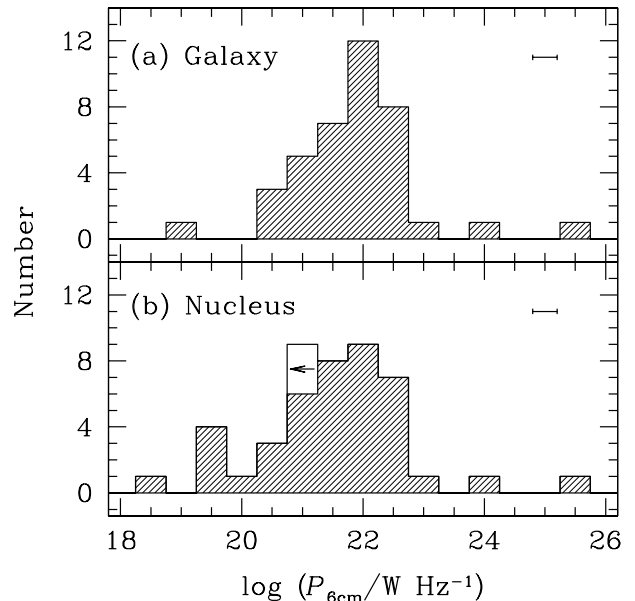


FIG. 1.— Distribution of monochromatic 6 cm radio power for (a) the integrated emission of the galaxy and (b) the AGN component alone. The open histograms denote upper limits. Typical error bars are shown (see § 3.3).

accommodate the most extreme spectral diversity observed (Elvis et al. 1994; Ho 1999b), the uncertainty in m_B can be as much as ~ 0.7 mag if the extrapolation is done from the *I* band. More typically the observations were conducted in *V*, and if $\Delta\alpha_o = \pm 0.5$, the uncertainty in m_B is only ~ 0.1 mag. (3) As in the radio band, variability introduces an uncertainty which is hard to quantify, but monitoring studies of Seyfert nuclei find that long-term flux variations are generally $\lesssim 0.5$ mag (e.g., Hamuy & Maza 1987; Winkler et al. 1992). (4) For lack of a secure handle on the effects of dust, we do not account for dust extinction from the host galaxy or internal to the nuclear region. Notwithstanding the “type 1” classification of our objects, the featureless continuum may be subject to non-negligible extinction. From their study of a hard X-ray selected sample of Seyfert 1s, Ward et al. (1987) argue that visual extinctions of $\sim 1\text{--}3$ mag are not uncommon. On the other hand, the conclusions of Ward et al. cannot be readily generalized to our optically selected sample, which may be biased toward less obscured sources. Winkler (1997) obtains $A_V \lesssim 1$ mag for the majority of a heterogeneous sample of 92 Seyfert 1s. (5) Finally, as with the radio emission, we assume that the point source entirely originates from the AGN, with minimal contribution from starlight. Although this is most likely not the case for every object, especially for the few where only ground-based spectrophotometry was available, it is probably not an unreasonable assumption given the high angular resolution of the *HST* images. Taking the above factors into consideration, we conservatively assign an uncertainty of 1 mag to our *B*-band nuclear magnitudes.

3. The uncertainties of the emission-line luminosities mainly arise from errors in flux calibration, aperture effects, variability, and extinction. The NLR extends over scales of at least tens to hundreds of parsecs, and therefore is partly resolved from the ground for nearby systems. Absolute spectrophotometry of extended objects is

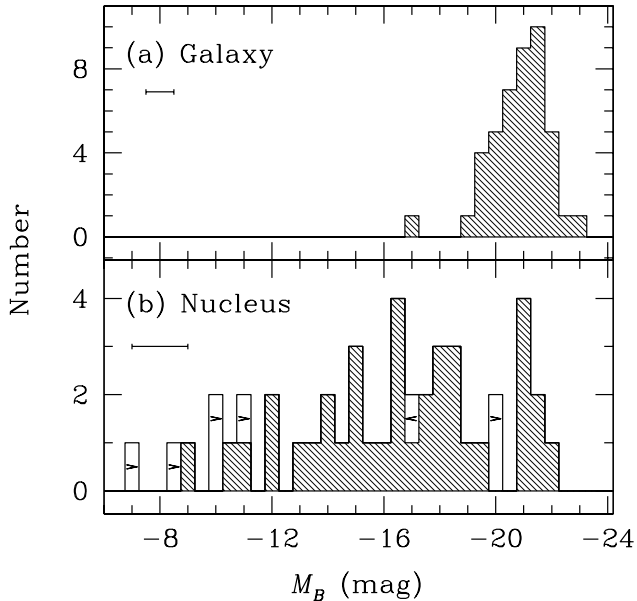


FIG. 2.— Distribution of absolute B magnitudes for (a) the integrated light of the galaxy and (b) the nucleus alone. The open histograms denote limits. Typical error bars are shown.

notoriously challenging without special effort, and aperture effects can be significant (see, e.g., discussion in Whittle 1992a). Flux errors of a factor of ~ 2 are not rare. It is relatively straightforward to estimate the extinction along the line of sight to the NLR; for the Palomar sample, the median $A_B \approx 0.6$ mag (§ 3.1). The situation for the BLR is more complicated (MacAlpine 1985), and no generally accepted method exists to estimate the extinction from optical spectra alone. Lastly, the broad-line emission in Seyferts varies in response to changes in the continuum level. We adopt a characteristic uncertainty of ± 0.3 dex for the [O III] and $H\beta$ luminosities.

4. RESULTS

4.1. Radio and Optical Luminosities

Figure 1 shows the distribution of monochromatic 6 cm radio powers. The top panel plots the integrated emission from the whole galaxy (host plus nucleus), which we approximate with low-resolution (beam $\gtrsim 1'$) measurements; the bottom panel isolates the nuclear contribution properly assigned to the AGN component. The two distributions are not dramatically different statistically. The AGN component on average accounts for $\sim 75\%$ of the integrated emission. However, the differences for any individual object *can* be very significant because the radio nuclear fraction varies from 0.01 to 1. The nuclear 6 cm radio powers range from $\sim 10^{18}$ to 10^{25} W Hz $^{-1}$, with a median value of $P_{6\text{cm}} = 1.6 \times 10^{21}$ W Hz $^{-1}$, after accounting for the small number of upper limits (Feigelson & Nelson 1985). This distribution is quite similar to that of Ho & Ulvestad (2001), who recently studied the entire sample of Seyferts (types 1 and 2) from the Palomar survey. The level of emission seen here is also comparable to that of radio cores detected in a large fraction of nearby elliptical and S0 galaxies (Sadler, Jenkins, & Kotanyi 1989; Wrobel & Heeschen 1991; Ho 1999a).

The contrast between the nuclear and integrated light is much more dramatic at optical wavelengths (Fig. 2). The

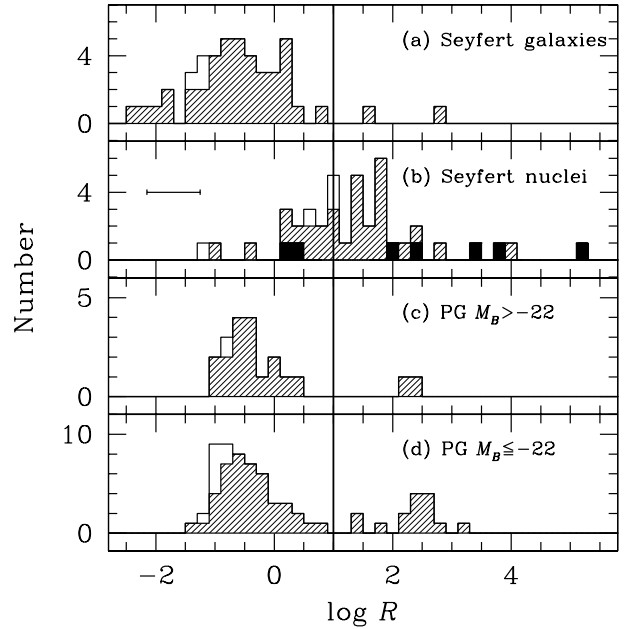


FIG. 3.— Distribution of the radio-to-optical luminosity ratio R for (a) the entire Seyfert galaxy, (b) the Seyfert nucleus alone, (c) PG sources with $M_B > -22$ mag, and (d) PG sources with $M_B \leq -22$ mag. Upper and lower limits are denoted by open and solid histograms, respectively. The formal division between radio-loud and radio-quiet objects is given by $R = 10$ (solid vertical line). A typical error bar for the Seyfert nuclei is shown in panel (b).

median integrated absolute magnitude is $M_{BT} = -20.8$, comparable to the value obtained for all the Seyferts in the Palomar survey (Ho et al. 1997b). The distribution of M_{BT} is rather narrow; the interquartile range is only 1.3 mag. This reflects the fact that Seyfert nuclei inhabit a preferred, relatively restricted range of Hubble types. In stark contrast, the nuclear magnitudes, properly decomposed from the bulge, span from $M_B^{\text{nuc}} \approx -9$ to -22 mag, with no discernible peak in the distribution. In the most extreme cases, the nucleus accounts for merely 0.01% of the integrated light. The weakest Seyfert 1 nuclei, which may be regarded as “mini-quasars,” are a factor of $\sim 10^8$ (20 magnitudes) less powerful than the most luminous quasars known — a truly astonishing range for a single astrophysical phenomenon. Treating the single lower limit (Mrk 471, slight saturated) as a detection, the median value of $M_B^{\text{nuc}} = -16.8$ mag, with an interquartile range of 4.7 mag. As expected, the CfA Seyferts are typically more luminous than the Palomar sources: median $M_B^{\text{nuc}} = -17.4$ mag vs. -14.6 mag. The two most luminous CfA Seyferts, I Zw 1 and Mrk 231, have absolute magnitudes which approach the conventional, albeit arbitrary, border between Seyferts and quasars ($M_B = -22$ mag, adjusted to $H_0 = 75$ km s $^{-1}$ Mpc $^{-1}$; Schmidt & Green 1983).

4.2. Radio-Loudness Parameter

Our reevaluation of the radio-loudness parameter for Seyferts appears in Figure 3. Not surprisingly, when R is computed using the integrated optical and radio emission of the entire galaxy (Fig. 3a), the vast majority of the objects lie to the left of the boundary demarcating the radio-quiet/radio-loud regimes. For a dividing line of

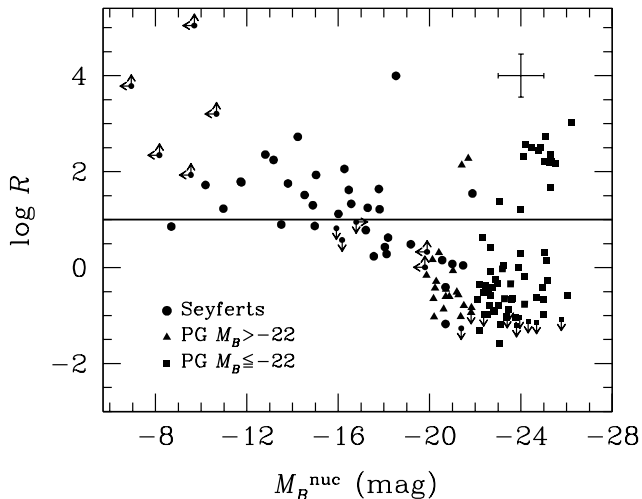


FIG. 4.— Distribution of nuclear R versus absolute B magnitude. Circles denote the Seyfert 1 nuclei from this study; triangles are PG sources with $M_B > -22$ mag; and squares are PG sources with $M_B \leq -22$ mag. Limits are indicated with arrows. The formal division between radio-loud and radio-quiet objects is given by $R = 10$ (solid horizontal line). A typical error bar for Seyfert nuclei is shown.

$R = 10$, the radio-loud fraction is 4%; the median value is $R \approx 0.2$. This is the result normally cited for Seyferts — most or all Seyferts are radio quiet. The values of R calculated using high-resolution measurements of the nuclei are shown in Figure 3b. Now the median value of $R \approx 17$ (treating the seven lower limits as detections), and the fraction of the sample which technically qualifies as radio-loud sources changes to $\gtrsim 60\%$. The majority (75%) of the objects lie between $R = 1$ and 100. This is the main result of this paper.

For comparison, we assembled equivalent data from the Palomar-Green (PG) quasar survey (Schmidt & Green 1983), as compiled by Kellermann et al. (1989). For consistency with our conventions, we recalculated the luminosities of the PG sources using $\alpha_r = -0.5$, $\alpha_o = -1.0$, $H_0 = 75 \text{ km s}^{-1} \text{ Mpc}^{-1}$, and $q_0 = 0.5$. With these parameters, 23% (20/87) of the PG objects have $M_B > -22$ mag and so can be deemed to be Seyfert 1 sources according to the definition of Schmidt & Green. As noted by Kellermann et al. (1989), the distribution of R shows no marked difference between the PG Seyferts (Fig. 3c) and the *bona fide* quasars (Fig. 3d). The PG sample, as do other optically selected quasar samples (e.g., Visnovsky et al. 1992; Hooper et al. 1995; Goldschmidt et al. 1999) exhibits a deficit of objects in the region $1 \lesssim R \lesssim 100$, which leads to an apparent bimodal distribution of R . The local Seyfert nuclei, interestingly, occupy precisely the “gap” created by the PG sources.

Nearby type 1 AGNs, with characteristically lower optical luminosities, populate a unique region of parameter space compared to more distant, more luminous sources: no object fainter than $M_B \approx -20$ mag has $R < 1$ (Fig. 4). The absence of points on the lower left portion of the diagram cannot be the result of selection effects because of the high detection rate in the radio (93%). Instead, it reflects the fact the strength of the radio and optical emission are broadly correlated over a very wide range of luminosities, as shown below.

4.3. Relation between Radio and Optical Luminosities

While the distribution of R values for Seyfert nuclei is neither bimodal, as is the case for the PG objects, nor sharply peaked, for the majority of the objects it does span a relatively restrictive range (factor ~ 100) over approximately four orders of magnitude in optical luminosity. This suggests that a correlation should exist between the radio and optical continuum luminosities. As shown in Figure 5a, a loose relation indeed is present between these two quantities. Interestingly, radio-loud and radio-quiet Seyferts lie on two slightly offset sequences, the extrapolations of which merge with similar sequences for the PG quasars. The radio-loud branch is steeper than the radio-quiet branch. Repeating the analysis by substituting the B -band continuum magnitudes with the [O III] (Fig. 5b) and H β (Fig. 5c) luminosities yields qualitatively very similar results.

Luminosity-luminosity correlations of the type shown in Figure 5 can be potentially misleading, since each of the variables itself correlates strongly with distance. A common practice is to reconsider the correlations in flux-flux space. As discussed by Feigelson & Berg (1983), however, such a procedure can lead to ambiguous results. Unless the two luminosities are linearly correlated, and unless upper limits are few or absent, the flux-flux plane may exhibit little or no correlation even if an intrinsically strong correlation is present in the luminosity-luminosity plane. The solution to safeguard against spurious distance effects is to perform a partial correlation analysis, taking distance as the third variable. In the case of censored data sets, Akritas & Siebert (1996) proposed the partial Kendall’s τ correlation test. Applying this test to our data, we verified that the statistical significance of the radio-optical correlations is high ($>99.9\%$; see Table 3). The correlations hold for Seyferts and quasars combined, for Seyferts alone, or for just radio-quiet quasars alone. The radio-loud quasars by themselves are not significantly correlated, probably because of the small number of objects.

To quantify the radio-optical relations, we calculated the linear regression coefficients using the method of Schmitt (1985), which treats censoring in both variables. The results are reported in Table 3. In Figure 5, we plot the regression lines separately for radio-loud and radio-quiet objects. Representing $L_{\text{radio}} \propto L_{\text{optical}}^a$, $a \approx 1.1$ –1.3 for radio-loud sources, and $a \approx 0.50$ –0.70 for radio-quiet sources.

4.4. Optical Continuum and Emission-Line Luminosity Correlation

Among the lines of evidence supporting the physical continuity between quasars and “classical” Seyfert nuclei, two historically important ones are (1) that the optical luminosities of the two classes overlap smoothly (Weedman 1976) and (2) that in both classes the optical nonstellar emission correlates strongly with the Balmer emission-line luminosity (Yee 1980; Shuder 1981). The latter observation, in particular, was instrumental in establishing photoionization as the principal mechanism for powering the optical line emission. Figure 6 revisits the relation between optical continuum and Balmer-line emission for type 1 AGNs. The PG sources follow a well defined

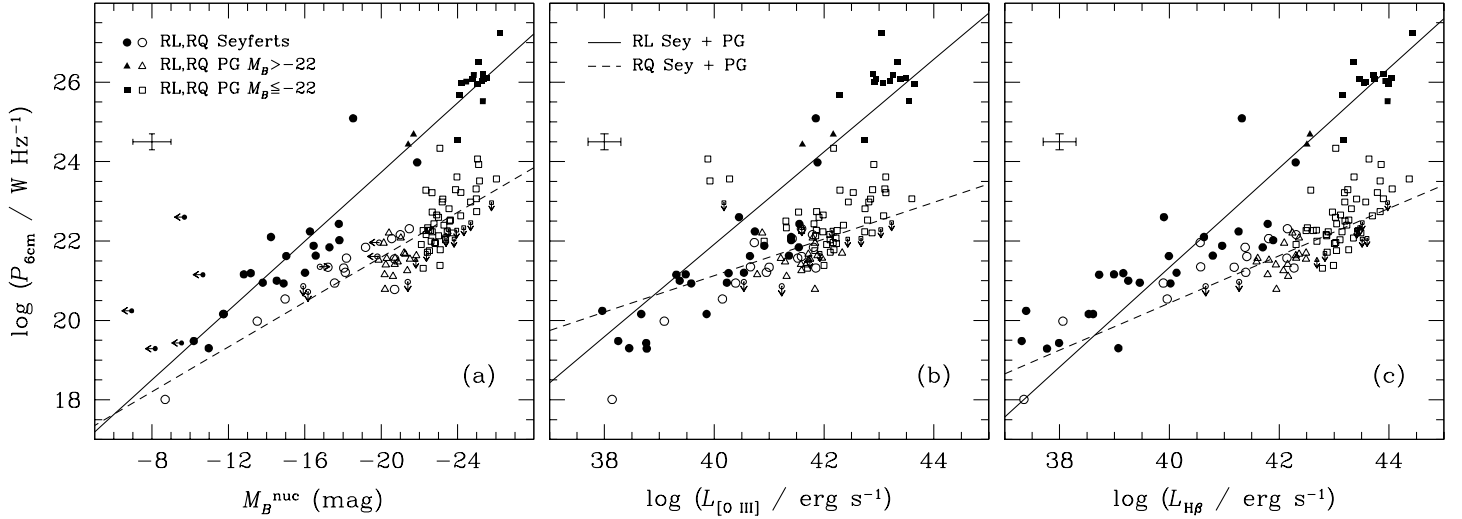


FIG. 5.— Correlations between nuclear monochromatic 6 cm radio power and (a) absolute B magnitude, (b) $[\text{O III}] \lambda 5007$ luminosity, and (c) $\text{H}\beta$ (broad + narrow components) luminosity. Circles denote the Seyfert 1 nuclei from this study; triangles are PG sources with $M_B > -22$ mag; and squares are PG sources with $M_B \leq -22$ mag. Radio-loud and radio-quiet sources are plotted with filled and open symbols, respectively, and arrows indicate limits. Significant Table 3) are shown for radio-loud (solid line) and radio-quiet (dashed line) objects. Typical error bars for Seyfert nuclei are shown.

relation between $\text{H}\beta$ luminosity and absolute B -band magnitude, roughly over $41.5 < \log L_{\text{H}\beta} < 44.5$ and $-20 \text{ mag} < M_B < -26 \text{ mag}$. The scatter is small, but non-negligible, as discussed by Miller et al. (1992). Albeit with considerably greater scatter, the local Seyferts extend the correlation to $\log L_{\text{H}\beta} \approx 38$ and $M_B \approx -8.0$ mag, approximately with the same slope and intercept defined by the quasars (see Table 3). The relation for Seyferts ($L_{\text{H}\beta} \propto L_B^{0.65}$) appears marginally shallower than that for quasars ($L_{\text{H}\beta} \propto L_B^{0.93}$), but we are unsure of the significance of the difference. The detection of broad emission lines, on which the type 1 Seyfert classification is based, becomes increasingly challenging for very low-luminosity objects (see Ho et al. 1997c). Thus, it is possible that the distribution of points toward the faint end of the $L_{\text{H}\beta} - M_B$ relation is biased toward higher values of $L_{\text{H}\beta}$, hence flattening the slope. Note that stellar contamination has the opposite effect: if the true nonstellar continuum in the Seyfert sample is less than we assume, the slope of the $L_{\text{H}\beta} - L_B$ relation would be even flatter. Radio-loud and radio-quiet objects lie on the same relation. The increased scatter for the low-luminosity sources may be largely due to the difficulty of the measurements (§ 3.3), but it could partly reflect *intrinsic* variations of physical conditions with luminosity. Two obvious possibilities are differences in the covering factor of the line-emitting gas and the spectral energy distribution. Recent work suggests that the broad-band spectra of low-luminosity AGNs deviate strongly from those of high-luminosity sources (Ho 1999b; Ho et al. 2000c).

As with the radio-optical relations (§ 4.3), the $L_{\text{H}\beta} - M_B$ correlation is statistically sound. After accounting for the mutual dependence of $L_{\text{H}\beta}$ and M_B on distance, the probability for accepting the null hypothesis that the two variables are uncorrelated is 7×10^{-4} for Seyferts and $< 10^{-8}$ for PG quasars (Table 3). The best-fitting linear regression

line for the combined sample, calculated using Schmitt’s (1985) method, is

$$\log L_{\text{H}\beta} = (-0.34 \pm 0.012)M_B + (35.1 \pm 0.25).$$

5. DISCUSSION

Active nuclei are commonplace in nearby galaxies, but they are nontrivial to study quantitatively. This paper demonstrates the importance of angular resolution in observations of Seyfert nuclei at radio and optical wavelengths. With its unprecedentedly broad luminosity coverage, our sample of objects pushes the Seyfert phenomenon to unfamiliar territories and leads us to reexamine a few longstanding issues.

5.1. The Radio-Loudness Paradigm

The physical processes underpinning the generation of radio sources remain central topics of discussion in the AGN community. Of particular interest is the origin of the apparent radio-loud/radio-quiet dichotomy. As discussed in the Introduction, Seyfert nuclei traditionally have been considered radio-quiet AGNs. This work emphasizes the difficulties that arise when trying to apply to Seyfert galaxies the conventional radio-loudness criterion. The standard measure of the relative luminosity in the radio and optical band is only meaningful when the photometric measurements pertain to the active nucleus. In the case of Seyferts, the nucleus often is dwarfed by the integrated emission from the host galaxy.

Our primary result, the distribution of nuclear R values for Seyfert 1 nuclei, challenges three pieces of popular wisdom: (1) that Seyfert galaxies are mainly radio-quiet objects; (2) that radio-loud AGNs are seldom found in disk galaxies; and (3) that the majority of AGNs are radio quiet. We find that at least 60% of our sample

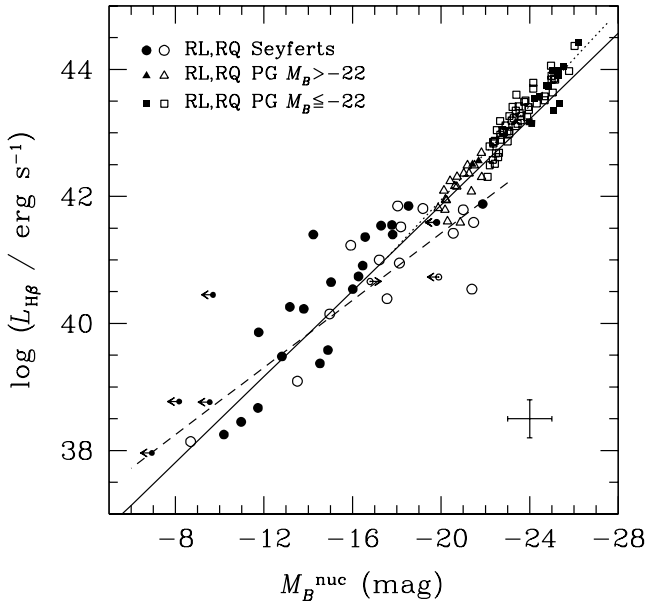


FIG. 6.— Correlation between nuclear H β (broad + narrow components) luminosity and absolute B magnitude. Symbols as in Figure 5. The best-fitting linear regressions are shown separately for all the objects (*solid line*), for the Seyferts alone (*dashed line*), and for the PG objects alone (*dotted line*). A typical error bar for Seyfert nuclei is shown.

of Seyferts technically qualify as radio-loud objects, and as Table 1 indicates, nearly all of them are spiral or S0 galaxies. The existence of radio-loud nuclei in disk galaxies has been discussed in related contexts by Ho (1999b) and Ho et al. (2000c). These remarks are not meant to undermine genuine differences that might exist between radio sources in Seyferts compared to those in more powerful AGNs. Most Seyferts have $R \approx 1 - 100$, values that straddle the two peaks in the R distribution of optically selected quasars, and they are certainly much less extreme than the R values seen in radio selected AGNs. Another feature which distinguishes Seyferts from typical radio-loud AGNs is the virtual absence of well collimated, large-scale jets. Seyferts do often possess linear radio structures reminiscent of jetlike outflows, but they occur exclusively on sub-galactic ($\lesssim 1$ kpc) scales (e.g., Ulvestad & Wilson 1989; Kukula et al. 1995; Ho & Ulvestad 2001). The scant available measurements of jet speeds suggest sub-relativistic motions (Ulvestad et al. 1998, 1999), although the first instance of superluminal jet motion in a Seyfert galaxy was recently reported by Brunthaler et al. (2000).

It is worth noting that although our definition of the radio-loudness parameter is widely used in the literature, it is by no means universally accepted. Miller et al. (1990) argue that the radio power alone should be regarded as a more fundamental discriminant. Their limiting criterion, $P_{6\text{cm}} \approx 10^{25} \text{ W Hz}^{-1} \text{ sr}^{-1}$, would exclude all but one of the objects in our sample, the well known radio source NGC 1275 (3C 84). However, we hold the perspective that the radio emission has physical significance in relation to the other sources of energy emanating from the central engine, and we consider the R parameter, which

captures the *relative* radiative output in the radio band, to be meaningful.⁶

5.2. Radio Emission and Accretion Rate

The connection between radio and optical emission has been much discussed in the context of quasars and powerful radio galaxies. The most widely reported correlations are those between radio power and optical narrow-line luminosity (e.g., Baum & Heckman 1989; Rawlings et al. 1989; Rawlings & Saunders 1991; Miller et al. 1993; McCarthy 1993; Tadhunter et al. 1998; Xu, Livio, & Baum 1999), broad-line luminosity (Celotti, Padovani, & Ghisellini 1997; Cao & Jiang 1999, 2001), and optical continuum luminosity (Miller et al. 1990; Stocke et al. 1992; Lonsdale, Smith, & Lonsdale 1995; Kukula et al. 1998; Serjeant et al. 1998).

We find that radio-quiet PG quasars obey strong correlations between radio power and three separate measures of optical luminosity (M_B , $L_{[\text{O III}]}$, $L_{\text{H}\beta}$), independent of distance effects. This confirms qualitatively similar findings in previous investigations of the PG sample (Stocke et al. 1992; Miller et al. 1993; Lonsdale et al. 1995). Radio-loud PG quasars do not follow these correlations, most likely because of the small sample size and its limited dynamic range in luminosity.

Seyfert nuclei form a natural extension of quasars in the radio-optical luminosity diagrams. Moreover, with our definition of the radio-loudness parameter, each of two radio classes plausibly follows its own correlation. Of the three radio-optical correlations for Seyferts, the best known is that involving the [O III] luminosity (de Bruyn & Wilson 1978; Whittle 1985, 1992b; Giuricin, Fadda, & Mezzetti 1996). Our results improve on the previous studies in several respects. First, our $P_{6\text{cm}} - L_{[\text{O III}]}$ diagram has virtually no upper limits. Second, its scatter is considerably reduced, most likely because of the high detection rate, the homogeneity of our sample, and the fact that we have restricted ourselves only to type 1 sources. Third, we (as do Giuricin et al.) explicitly account for distance effects. And fourth, we expand on the dynamic range of the luminosities, not only toward weaker sources but also connecting with the quasar domain.

The radio power correlates with H β luminosity with equal, and possibly even better, significance compared to $L_{[\text{O III}]}$. Baum & Heckman (1989) and Ho (1999a) have noted that Seyferts do exhibit a loose correlation between radio and H α luminosity, but that their locus lies offset from that formed by powerful radio galaxies. By contrast, the “radio-loud” Seyferts in our sample are not inconsistent with a simple extrapolation of the radio-loud PG quasars (Fig. 5c).

Published studies of the relationship between the radio and optical continuum luminosities of Seyferts give mixed, and at times conflicting, accounts. The integrated optical luminosities do correlate with radio power (Isobe, Feigelson, & Nelson 1986; Edelson 1987; Giuricin et al. 1990), but evidently *not* when distance effects are considered (Giuricin et al. 1996). Giuricin et al. (1996) collected ground-based nuclear magnitudes for a

⁶Rush et al. (1996) and Thean et al. (2000) have evaluated the radio-loudness of Seyfert galaxies according to the relative luminosities in the radio and far-infrared bands. The far-infrared data, however, are based on low-resolution measurements obtained with *IRAS*, and thus suffer severe contamination from the host galaxy.

TABLE 3: STATISTICAL RESULTS

Variables		Subsample				Correlation			Regression	
X (1)	Y (2)	Objects (3)	N (4)	N_{ul}^X (5)	N_{ul}^Y (6)	τ (7)	σ (8)	P_{null} (9)	$a \pm \sigma_a$ (10)	$b \pm \sigma_b$ (11)
M_B^{uc}	$\log P_{6cm}$	(A) All Sey1	45	7	3	-0.198	0.0753	8.6×10^{-3}	-0.24 ± 0.047	17.33 ± 0.76
M_B^{uc}	$\log P_{6cm}$	(B) RL Sey1	25	5	0	-0.299	0.0812	2.3×10^{-4}	-0.35 ± 0.087	16.20 ± 1.30
M_B^{uc}	$\log P_{6cm}$	(C) RQ Sey1	20	2	3	-0.479	0.147	1.1×10^{-3}	-0.27 ± 0.045	16.21 ± 0.84
M_B^{uc}	$\log P_{6cm}$	(D) All PG	87	0	9	-0.274	0.0689	6.9×10^{-5}		
M_B^{uc}	$\log P_{6cm}$	(E) RL PG	16	0	0	-0.475	0.302	1.2×10^{-1}		
M_B^{uc}	$\log P_{6cm}$	(F) RQ PG	71	0	9	-0.262	0.0572	4.7×10^{-7}	-0.29 ± 0.031	15.72 ± 0.69
M_B^{uc}	$\log P_{6cm}$	(G) RL Sey1+PG	41	5	3	-0.323	0.0974	9.1×10^{-4}	-0.44 ± 0.018	15.01 ± 0.34
M_B^{uc}	$\log P_{6cm}$	(H) RQ Sey1+PG	91	2	12	-0.246	0.0451	5.9×10^{-8}	-0.28 ± 0.021	15.94 ± 0.44
$\log L_{[O III]}$	$\log P_{6cm}$	(A) All Sey1	42	0	2	0.356	0.0877	4.9×10^{-5}	0.67 ± 0.097	-5.72 ± 3.85
$\log L_{[O III]}$	$\log P_{6cm}$	(B) RL Sey1	25	0	0	0.424	0.115	2.2×10^{-4}	0.79 ± 0.10	-9.98 ± 3.94
$\log L_{[O III]}$	$\log P_{6cm}$	(C) RQ Sey1	17	0	2	0.394	0.145	6.7×10^{-3}	0.62 ± 0.14	-4.05 ± 5.61
$\log L_{[O III]}$	$\log P_{6cm}$	(D) All PG	87	0	9	0.254	0.0612	3.3×10^{-5}		
$\log L_{[O III]}$	$\log P_{6cm}$	(E) RL PG	16	0	0	0.098	0.154	5.3×10^{-1}		
$\log L_{[O III]}$	$\log P_{6cm}$	(F) RQ PG	71	0	9	0.165	0.0808	4.1×10^{-2}	0.15 ± 0.19	16.04 ± 7.84
$\log L_{[O III]}$	$\log P_{6cm}$	(G) RL Sey1+PG	41	0	0	0.359	0.0957	1.8×10^{-4}	1.16 ± 0.068	-24.65 ± 2.76
$\log L_{[O III]}$	$\log P_{6cm}$	(H) RQ Sey1+PG	88	0	11	0.193	0.0683	4.7×10^{-3}	0.46 ± 0.15	2.68 ± 6.21
$\log L_{H\beta}$	$\log P_{6cm}$	(A) All Sey1	42	0	2	0.471	0.106	9.2×10^{-6}	0.87 ± 0.14	-13.69 ± 5.52
$\log L_{H\beta}$	$\log P_{6cm}$	(B) RL Sey1	25	0	0	0.526	0.135	1.0×10^{-4}	1.03 ± 0.15	-19.86 ± 5.97
$\log L_{H\beta}$	$\log P_{6cm}$	(C) RQ Sey1	17	0	2	0.460	0.177	9.5×10^{-3}	0.89 ± 0.19	-14.97 ± 7.91
$\log L_{H\beta}$	$\log P_{6cm}$	(D) All PG	87	0	9	0.209	0.0609	5.9×10^{-4}		
$\log L_{H\beta}$	$\log P_{6cm}$	(E) RL PG	16	0	0	0.241	0.329	4.6×10^{-1}		
$\log L_{H\beta}$	$\log P_{6cm}$	(F) RQ PG	71	0	9	0.241	0.0504	1.7×10^{-6}	0.72 ± 0.096	-8.84 ± 4.10
$\log L_{H\beta}$	$\log P_{6cm}$	(G) RL Sey1+PG	41	0	0	0.486	0.151	1.3×10^{-3}	1.25 ± 0.055	-28.84 ± 2.31
$\log L_{H\beta}$	$\log P_{6cm}$	(H) RQ Sey1+PG	88	0	11	0.236	0.0496	1.9×10^{-6}	0.59 ± 0.083	-3.38 ± 3.49
M_B^{uc}	$\log L_{H\beta}$	(A) All Sey1	42	7	0	-0.325	0.0959	7.0×10^{-4}	-0.26 ± 0.033	36.13 ± 0.54
M_B^{uc}	$\log L_{H\beta}$	(D) All PG	87	0	0	-0.589	0.0920	$< 1.0 \times 10^{-8}$	-0.37 ± 0.015	34.53 ± 0.34
M_B^{uc}	$\log L_{H\beta}$	(I) All Sey1+PG	129	7	0	-0.413	0.0598	$< 1.0 \times 10^{-8}$	-0.34 ± 0.012	35.11 ± 0.25

NOTE.— Col. (1) Variable X . Col. (2) Variable Y . Col. (3) Subsample. Col. (4) Number of objects in the subsample. Col. (5) Number of upper limits in variable X . Col. (6) Number of upper limits in variable Y . Col. (7)–(9) Results of partial correlation analysis which takes into account mutual correlations of X and Y with redshift, giving the partial Kendall's τ correlation coefficient, the square root of the calculated variance σ , and the associated probability P_{null} for accepting the null hypothesis that there is no correlation. Col. (10)–(11) Results of Schmitt's binned linear regression, $Y = (a \pm \sigma_a)X + (b \pm \sigma_b)$.

heterogeneous sample of Seyfert 1 nuclei, and these, too, were found to be intrinsically decoupled from the radio powers. Our sample, on the contrary, shows a strong, intrinsic correlation between P_{6cm} and M_B (Fig. 5a). In fact, we suggest that separate $P_{6cm} - M_B$ relations can be defined for each of the two radio classes of Seyferts and quasars combined. The discrepant results of Giuricin et al. (1996) perhaps stem from the large fraction of upper limits in their sample ($\sim 60\%$ for both radio and optical luminosities), the inhomogeneous sources of published measurements they used, or residual contamination of host-galaxy emission in their ground-based optical data. That Seyferts and radio-quiet quasars share a single radio-optical continuum correlation was first proposed by Kukula et al. (1998), who compared the Seyfert 1s from the CfA sample with a subset of 27 low-redshift PG sources. To mitigate host-galaxy contamination for the Seyferts, Kukula et al. utilized ground-based “nuclear” magnitudes from Huchra & Burg (1992). Two caveats, however, can be raised against the analysis of Kukula et al. First, they did not consider the effect of distance on the correlation. And second, as these authors recognized, their correction

for host-galaxy light yields only crude AGN magnitudes, since Huchra & Burg's photometry was based on apertures of diameters $\gtrsim 10''$ – $15''$.

Although the empirical case for the reality of the various radio-optical correlations seems secure, the physical basis behind them is less transparent. In the case of Seyferts, the correlations between radio power and both the kinematics (Wilson & Willis 1980; Whittle 1985) and luminosity (see above) of the NLR have long implicated a strong coupling between the energetics of the relativistic plasma and the narrow-line gas (de Bruyn & Wilson 1978). The correlations presented in Figure 5 inject a fresh perspective into the discussion. The radio power does not correlate *just* with the NLR ([O III]) luminosity, but at least as well with the nonstellar continuum and the BLR luminosity (included in $L_{H\beta}$). In fact, all three radio-optical correlations exhibit approximately the same form and scatter. This suggests that there may be a single underlying cause.

The simplest interpretation is that the accretion rate directly influences the fueling of relativistic radio jets, as invoked in certain models (e.g., Falcke & Biermann 1995; Xu et al. 1999, and references therein). Among the three

measures of the optical luminosity we have considered, the nonstellar continuum may be regarded as the most “fundamental.” We assume, as is customary, that the featureless optical continuum represents the low-energy tail of the ionizing spectrum produced by the central accretion disk. Photoionization then powers the BLR and NLR emission, which we measure by $H\beta$ and [O III]. Indeed, the $L_{H\beta} - M_B$ relation (§ 4.4) supports this scenario. Thus, to the extent that M_B , $L_{[O III]}$, and $L_{H\beta}$ each traces the accretion luminosity, which scales linearly with the mass accretion rate for an optically thick, geometrically thin disk, all three optical luminosities are equivalent.

5.3. Low-Luminosity AGNs

Although the physical nature of Seyfert nuclei normally is not controversial, some of the objects in our sample have such extremely low luminosities that their status as “AGNs” may seem questionable. Indeed, the objects at the faint end of the luminosity distribution are no brighter than single supergiant stars. Apart from the presence of a BLR, as implied by the detection of broad emission lines, this study, in conjunction with that of Ho & Ulvestad (2001), furnishes several other pieces of evidence which help to establish a physical continuity between low-luminosity Seyfert nuclei and more luminous AGNs. (1) Compact radio cores are detected nearly ubiquitously, often accompanied by linear features morphologically akin to radio jets. (2) Judging from their radio-to-optical luminosity ratios, a substantial fraction of the sources are “radio-loud,” a trait normally associated with the AGN phenomenon. (3) The radio power scales with three measures of the optical power (continuum, [O III], and $H\beta$ emission) and merges continuously with the quasar population. (4) Lastly, a strong relation exists between optical continuum luminosity and $H\beta$ luminosity, covering nearly seven orders of magnitude in each variable. Terashima, Ho, & Ptak (2000) and Ho et al. (2001a), using hard X-ray observations, recently arrived at similar conclusions for related classes of low-luminosity nuclei. These findings support the hypothesis that AGNs with a remarkably broad range of power, ranging from quasars to classical Seyferts to ultra low-luminosity nuclei, are regulated by similar basic physical processes.

6. SUMMARY

We present radio and optical photometry for the nuclear regions of a well defined sample of 45 nearby Seyfert 1 galaxies to investigate the relationship between the emission in these two bands. We emphasize the importance of high angular resolution to properly isolate the AGN com-

ponent from the contaminating bright background of the host galaxy. These data are supplemented with similar measurements for the subset of 87 Palomar-Green quasars with redshifts less than 0.5, allowing us to assemble a sizable sample of type 1 AGNs which covers nearly seven orders of magnitude in radio and optical luminosity. Our principal conclusions are the following:

- The nuclear radio-to-optical luminosity ratios of Seyfert 1 nuclei largely range from $R \approx 1$ to 100. At least 60% of the sources are characterized by $R \geq 10$, a territory traditionally reserved for radio-loud AGNs. This finding dispels the popular notion that most Seyferts, and by implication their spiral hosts, are radio-quiet objects.
- Seyfert 1 nuclei and optically selected quasars collectively display strong, intrinsic correlations between radio and optical power, the latter including non-stellar continuum, [O III], and $H\beta$ luminosity. Separate correlations can be defined for radio-loud and radio-quiet sources.
- The physical origin underlying the radio-optical correlations may be a close link between the disk accretion rate and the generation of relativistic radio jets.
- The relation between optical continuum and Balmer-line luminosity extends from $M_B \approx -26$ mag to $M_B \approx -8$ mag.
- The physical processes responsible for the production of radio and optical emission in low-luminosity Seyfert nuclei are closely related to those in classical Seyferts and quasars.

We thank J. S. Ulvestad, A. V. Filippenko, and W. L. W. Sargent for permission to use data in advance of publication, J. J. Condon, the referee, for helpful comments, and D. L. Meier for insights on jet physics. The research of L. C. H. is supported by NASA grants HST-GO-06837.04-A, HST-AR-07527.03-A, and HST-AR-08361.02-A, awarded by the Space Telescope Science Institute, which is operated by AURA, Inc., under NASA contract NAS5-26555. This work made use of the NASA/IPAC Extragalactic Database (NED) which is operated by the Jet Propulsion Laboratory, California Institute of Technology, under contract with NASA.

REFERENCES

- Adams, T. F. 1977, ApJS, 33, 19
 Akritas, M. G., & Siebert, J. 1996, MNRAS, 278, 919
 Baum, S. A., & Heckman, T. M. 1989, ApJ, 336, 702
 Becker, R. H., White, R. L., & Edwards, A. L. 1991, ApJS, 75, 1
 Blandford, R. D. 1990, in Active Galactic Nuclei, SAAS-FEE Advanced Course 20, Swiss Society for Astrophysics and Astronomy, ed. T. J.-L. Courvoisier & M. Mayor (Berlin: Springer), 161
 Boroson, T. A., & Green, R. F. 1992, ApJS, 80, 109
 Brunthaler, A., Falcke, H., Bower, G. C., Aller, M. F., Aller, H. D., Teräsranta, H., Lobanov, A. P., Krichbaum, T. P., & Patnaik, A. R. 2000, A&A, 357, L45
 Cao, X., & Jiang, D. R. 1999, MNRAS, 307, 802
 ——. 2001, MNRAS, 320, 347
 Cardelli, J. A., Clayton, G. C., & Mathis, J. S. 1989, ApJ, 345, 245
 Carollo, C. M., Stiavelli, M., de Zeeuw, P. T., & Mack, J. 1997, AJ, 114, 2366
 Celotti, A., Padovani, P., & Ghisellini, G. 1997, MNRAS, 286, 415
 Condon, J. J. 1987, ApJS, 65, 485
 Condon, J. J., Condon, M. A., Gisler, G., & Puschell, J. J. 1982, ApJ, 252, 102
 Condon, J. J., Huang, Z.-P., Yin, Q. F., & Thuan, T. X. 1991, ApJ, 378, 65
 Cruz-González, I., Carrasco, L., Serrano, A., Guichard, J., Dultzin-Hacyan, D., & Bisiacchi, G. F. 1994, ApJS, 94, 47
 Dahari, O., & De Robertis, M. M. 1988, ApJS, 67, 249

- de Bruyn, A. G., & Wilson, A. S. 1978, *A&A*, 64, 433
- Della Ceca, R., Palumbo, G. G. C., Persic, M., Boldt, E. A., Marshall, E. E., & De Zotti, G. 1990, *ApJS*, 72, 471
- de Vries, W. H., O'Dea, C. P., Barthel, P. D., Fanti, C., Fanti, R., & Lehnert, M. D. 2000, *AJ*, 120, 2300
- Edelson, R. 1987, *ApJ*, 313, 651
- Elvis, M., Wilkes, B. J., McDowell, J. C., Green, R. F., Bechtold, J., Willner, S. P., Oey, M. S., Polomski, E., & Cutri, R. 1994, *ApJS*, 95, 1
- Falcke, H., & Biermann, P. L. 1995, *A&A*, 293, 665
- Feigelson, E. D., & Berg, C. J. 1983, *ApJ*, 269, 400
- Feigelson, E. D., & Nelson, P. I. 1985, *ApJ*, 293, 192
- Filho, M. E., Barthel, P. D., & Ho, L. C. 2000, *ApJS*, 129, 93
- Filippenko, A. V., & Sargent, W. L. W. 1989, *ApJ*, 342, L11
- Gaskell, C. M., & Ferland, G. J. 1984, *PASP*, 96, 393
- Giuricin, G., Fadda, D., & Mezzetti, M. 1996, *ApJ*, 468, 475
- Giuricin, G., Mardirossian, F., Mezzetti, M., & Bertotti, G. 1990, *ApJS*, 72, 551
- Goldschmidt, P., Kukula, M. J., Miller, L., & Dunlop, J. S. 1999, *ApJ*, 511, 612
- Goodrich, R. W., & Osterbrock, D. E. 1983, *ApJ*, 269, 416
- Green, R. F., Schmidt, M., & Liebert, J. 1986, *ApJS*, 61, 305
- Halpern, J. P., & Steiner, J. E. 1983, *ApJ*, 269, L37
- Hamilton, T. S., Casertano, S., & Turnshek, D. A. 2001, *ApJ*, in press
- Hamuy, M., & Maza, J. 1987, *A&AS*, 68, 383
- Ho, L. C. 1999a, *ApJ*, 510, 631
- 1999b, *ApJ*, 516, 672
- Ho, L. C., et al. 2001a, *ApJ*, in press
- Ho, L. C., Filippenko, A. V., & Sargent, W. L. W. 1995, *ApJS*, 98, 477
- 1996, *ApJ*, 462, 183
- 1997a, *ApJS*, 112, 315
- 1997b, *ApJ*, 487, 568
- Ho, L. C., Filippenko, A. V., Sargent, W. L. W., & Peng, C. Y. 1997c, *ApJS*, 112, 391
- Ho, L. C., Rudnick, G., Rix, H.-W., Shields, J. C., McIntosh, D. H., Filippenko, A. V., Sargent, W. L. W., & Eracleous, M. 2000c, *ApJ*, 541, 120
- Ho, L. C., & Ulvestad, J. S. 2001, *ApJS*, in press
- Ho, L. C., Van Dyk, S. D., Pooley, G. G., Sramek, R. A., & Weiler, K. W. 1999, *AJ*, 118, 843
- Holtzman, J., et al. 1995, *PASP*, 107, 1065
- Hooper, E. J., Impey, C. D., Foltz, C. B., & Hewett, P. C. 1995, *ApJ*, 445, 62
- Huchra, J. P., & Burg, R. 1992, *ApJ*, 393, 90
- Huchra, J. P., Davis, M., Latham, D., & Tonry, J. 1983, *ApJS*, 52, 89
- Hummel, E. 1981, *A&A*, 93, 93
- Isobe, T., Feigelson, E. D., & Nelson, P. I. 1986, *ApJ*, 306, 490
- Kellermann, K. I., Sramek, R. A., Schmidt, M., Green, R. F., Shaffer, D. B. 1994, *AJ*, 108, 1163
- Kellermann, K. I., Sramek, R. A., Schmidt, M., Shaffer, D. B., & Green, R. F. 1989, *AJ*, 98, 1195
- Krolik, J. H. 1998, *Active Galactic Nuclei* (Princeton: Princeton Univ. Press)
- Kukula, M. J., Dunlop, J. S., Hughes, D. H., & Rawlings, S. 1998, *MNRAS*, 297, 366
- Kukula, M. J., Pedlar, A., Baum, S. A., O'Dea, C. P. 1995, *MNRAS*, 276, 1262
- Laor, A. 2000, *ApJ*, 543, L111
- Lawrence, A. 1987, *PASP*, 99, 309
- Lonsdale, C. J., Smith, H. E., & Lonsdale, C. J. 1995, *ApJ*, 438, 632
- MacAlpine, G. M. 1985, in *Astrophysics of Active Galaxies and Quasi-Stellar Objects*, ed. J. S. Miller (Mill Valley, CA: Univ. Science Books), 259
- MacKenty, J. W. 1990, *ApJS*, 72, 231
- Malkan, M. A., Gorjian, V., & Tam, R. 1998, *ApJS*, 117, 25
- Matthews, T. A., Morgan, W. W., & Schmidt, M. 1964, *ApJ*, 140, 35
- McCarthy, P. J. 1993, *ARA&A*, 31, 639
- McLure, R. J., Dunlop, J. S., Kukula, M. J., Baum, S. A., O'Dea, C. P., & Hughes, D. H. 1999, *MNRAS*, 308, 377
- Meurs, E. J. A., & Wilson, A. S. 1984, *A&A*, 136, 206
- Miller, L., Peacock, J. A., & Mead, A. R. G. 1990, *MNRAS*, 244, 207
- Miller, P., Rawlings, S., & Saunders, R. 1993, *MNRAS*, 263, 425
- Miller, P., Rawlings, S., Saunders, R., & Eales, S. 1992, *MNRAS*, 254, 93
- Morris, S. L., & Ward, M. J. 1988, *MNRAS*, 230, 639
- Mushotzky, R. F., & Wandel, A. 1989, *ApJ*, 339, 674
- Nandra, K., George, I. M., Mushotzky, R. F., Turner, T. J., & Yaqoob, T. 1997, *ApJ*, 477, 602
- Nelson, C. H., MacKenty, J. W., Simkin, S. M., & Griffiths, R. E. 1996, *ApJ*, 466, 713
- Niklas, S., Klein, U., & Wielebinski, R. 1995, *A&A*, 293, 56
- Osterbrock, D. E. 1981, *ApJ*, 249, 462
- 1984, *QJRAS*, 25, 1
- Osterbrock, D. E., & Martel, A. 1993, *ApJ*, 414, 552
- Peterson, B. M. 1997, *An Introduction to Active Galactic Nuclei* (Cambridge: Cambridge Univ. Press)
- Phillips, A. C., Illingworth, G. D., MacKenty, J. W., & Franx, M. 1996, *AJ*, 111, 1566
- Ravindranath, S., Ho, L. C., Peng, C. Y., Filippenko, A. V., & Sargent, W. L. W. 2001, *AJ*, submitted
- Rawlings, S., & Saunders, R. 1991, *Nature*, 349, 138
- Rawlings, S., Saunders, R., Eales, S. A., & Mackay, C. D. 1989, *MNRAS*, 240, 701
- Rush, B., Malkan, M. A., & Edelson, R. A. 1996, *ApJ*, 473, 130
- Sadler, E. M., Jenkins, C. R., & Kotanyi, C. G. 1989, *MNRAS*, 240, 591
- Schlegel, D. J., Finkbeiner, D. P., & Davis, M. 1998, *ApJ*, 500, 525
- Schmidt, M., & Green, R. F. 1983, *ApJ*, 269, 352
- Schmitt, J. H. M. M. 1985, *ApJ*, 293, 178
- Serjeant, S., Rawlings, S., Maddox, S. J., Baker, J. C., Clements, D., Lacy, M., & Lilje, P. B. 1998, *MNRAS*, 294, 494
- Shuder, J. M. 1981, *ApJ*, 244, 12
- Sramek, R. A., & Weedman, D. W. 1980, *ApJ*, 238, 435
- Stirpe, G. M., et al. 1994, *A&A*, 285, 857
- Stocke, J. T., Morris, S. L., Weymann, R. J., & Foltz, C. B. 1992, *ApJ*, 396, 487
- Strittmatter, P. A., Hill, P., Pauliny-Toth, I. I. K., Steppe, H., & Witzel, A. 1980, *A&A*, 88, L12
- Tadhunter, C. N., Morganti, R., Robinson, A., Dickson, R., Villar-Martín, M., & Fosbury, R. A. E. 1998, *MNRAS*, 298, 1035
- Terashima, Y., Ho, L. C., & Ptak, A. F. 2000, *ApJ*, 539, 161
- Thean, A., Pedlar, A., Kukula, M. J., Baum, S. A., & O'Dea, C. P. 2000, *MNRAS*, 314, 573
- Tully, R. B. 1988, *Nearby Galaxies Catalog* (Cambridge: Cambridge Univ. Press)
- Ulvestad, J. S. 1986, *ApJ*, 310, 136
- Ulvestad, J. S., Roy, A. L., Colbert, E. J. M., & Wilson, A. S. 1998, *ApJ*, 496, 196
- Ulvestad, J. S., & Wilson, A. S. 1984a, *ApJ*, 278, 544
- 1984b, *ApJ*, 285, 439
- 1989, *ApJ*, 343, 659
- Ulvestad, J. S., Wrobel, J. M., Roy, A. L., Wilson, A. S., Falcke, H., & Krichbaum, T. P. 1999, *ApJ*, 517, L81
- Visnovsky, K. L., Impey, C. D., Foltz, C. B., Hewett, P. C., Weymann, R. J., & Morris, S. L. 1992, *ApJ*, 391, 560
- Wadadekar, Y., & Kembhavi, A. 1999, *AJ*, 118, 1435
- Ward, M., Elvis, M., Fabbiano, G., Carleton, N. P., Willner, S. P., & Lawrence, A. 1987, *ApJ*, 315, 74
- Weedman, D. W. 1976, *ApJ*, 208, 30
- White, R. L., et al. 2000, *ApJS*, 126, 133
- Whittle, M. 1985, *MNRAS*, 213, 33
- 1992a, *ApJS*, 79, 49
- 1992b, *ApJ*, 387, 109
- Wilson, A. S., & Willis, A. J. 1980, *ApJ*, 240, 429
- Winkler, H. 1997, *MNRAS*, 292, 273
- Winkler, H., Glass, I. S., van Wyk, F., Marang, F., Jones, J. H. S., Buckley, D. A. H., & Sekiguchi, K. 1992, *MNRAS*, 257, 659
- Wrobel, J. M. 2000, *ApJ*, 531, 716
- Wrobel, J. M., & Heeschen, D. S. 1991, *AJ*, 101, 148
- Xu, C., Livio, M., & Baum, S. A. 1999, *AJ*, 118, 1169
- Yee, H. K. C. 1980, *ApJ*, 241, 894
- 1983, *ApJ*, 272, 473
- Zirbel, E. L. 1996, *ApJ*, 473, 713